Fractal and Multifractal Characterization of Stochastic Fracture Networks and Real Outcrops

Weiwei Zhu[a], Gang Lei[b], Xupeng He[c], Tad W. Patzek[c], Moran Wang[a,*]

[a] *Tsinghua University, Beijing, China*
[b] *China University of Geosciences, Wuhan, China*
[c] *Ali I. Al-Naimi Petroleum Engineering Research Center (ANPERC), King Abdullah University of Science and Technology, Thuwal, KSA*

Abstract

The fractal dimension and multifractal spectrum are widely used to characterize the complexity of natural fractures. However, a systematic investigation on the impact of different fracture properties (fracture lengths, orientations, center positions, system sizes) on fractal and multifractal characterization of complex fracture networks is missing. We utilize an in-house developed DFN modeling software, HatchFrac, to construct stochastic fracture networks with prescribed distributions and systematically study the impact of four geometrical properties of fractures on the fractal and multifractal characterization. We calculate the single fractal dimension and multifractal spectrum with the box-counting method. The single fractal dimension, D, and the difference of singularity exponent, $\Delta\alpha$, are used to represent the fractal and multifractal patterns, respectively. We find that fracture lengths, orientations and system sizes have positive correlations with D and $\Delta\alpha$, while the system size has the most significant impact among the four parameters. D is uncorrelated with fracture positions (F_D), which means that a single fractal dimension cannot capture the complexity caused by clustering effects. However, $\Delta\alpha$ has a strong negative correlation with F_D, which implies that clustering effects make fracture networks more complex, and $\Delta\alpha$ can capture the difference. We also digitize

*Moran Wang
Email address: mrwang@tsinghua.edu.cn (Moran Wang)

60 outcrop maps with a novel fracture detection algorithm and calculate their fractal dimension and multifractal spectrum. We find wide variations of D and $\Delta\alpha$ on those outcrop maps, even for outcrops at similar scales. It means that a universal indicator for characterizing fracture networks at different scales or the same scale is almost impossible.

1. Introduction

Fractures such as joints, faults, pressure solution seams, and deformation bands are ubiquitous in crustal rocks. Natural fractures usually comprise complex networks, and they vary in size over scales ranging from microns to hundreds of kilometres [1, 2]. Throughout this large scale range, fracture networks dominate the geomechanical and hydrological behavior of subsurface rocks and play an essential role in many engineering fields, e.g., hydrology, waste disposal, earthquakes, petroleum and geothermal reservoir exploitation [3, 4, 5, 6].

Mandelbrot [7] proposed the concept of fractals, which can be used to characterize irregular sets, regardless of the scale at which these sets are examined. Many researchers have investigated the fractal behaviors of natural fractures from outcrop observations and experiments. Otsuki and Dilov [8], Shi et al. [9] and Wu et al. [10] found the fractal pattern of fractures in millimeter scales through experiments and micro-CT images, while Okubo and Aki [11],Matsumoto et al. [12],Aviles et al. [13], and Cello [14] investigated complex structures of large scale faults with fractal dimensions, e.g., San Andreas fault. Barton [15] collected 17 outcrop maps from various tectonic settings, lithologies and scales and analyzed their fractal dimension. However, a single fractal dimension is insufficient to describe fracture systems with complex geometrical patterns, including orientation distribution, size population and fracture trace geometry [16, 17]. Instead, multifractals describe sets comprising a union of fractal subsets, each identified by specific measure and characterized by different fractal dimension [18]. The first characterization of multifractals was introduced by Mandelbrot [19]. Frisch and Parisi [20] and Halsey et al. [21] further

developed the formalism. Cowie et al. [22] found strongly multifractal properties through numerical models that simulated fracture growth in a tectonic plate. Berkowitz and Hadad [18] introduced in detail the fractal and multifractal descriptions of complex fracture networks and analyzed the multifractal characterization of synthetic fracture networks. However, in their research, generated synthetic fracture networks did not cover a wide range of their geometry distributions, which leads to incomplete conclusions.

Fractals and multifractals are used to characterize the complexity of fracture systems. However, a detailed investigation of the impact of different fracture properties, e.g., fracture length, orientations, and center positions, on the fractal characterizations of complex fracture networks is missing. One main possible reason is that obtaining enough geological data with systematically different fracture patterns is almost impossible. The only practical alternative is the discrete fracture network (DFN) modeling method, which preserves essential geometric and topological structures of fractures. A "discrete fracture network" (DFN) refers to a computational model that explicitly represents the geometrical properties of individual fracture, which mainly includes orientation, size, position, shape, and aperture [23]. With the powerful in-house developed discrete fracture network modeling software, HatchFrac [24, 25], we can generate a large number of fracture networks with prescribed property distributions.

In this research, we systematically investigate the impact of essential fracture geometry descriptors, including fracture lengths, orientations, center positions and system sizes, on the fractal and multifractal characterization of stochastic fracture networks. Furthermore, we digitize 60 real outcrop maps using a novel pixel-based fracture detection algorithm [26] and investigate their fractal and multifractal patterns.

The conventional method of fractal analysis of fracture networks is the box-counting technique [15], based on the outcrop images. Roy et al. [27] proposed an improved box-counting method and argued that there is a limiting box size because fracture images have a finite resolution. In this research, DFN models represent fractures with line segments, and the fracture detection algorithm can

automatically interpret fractures as line segments or polylines. Therefore, limits on the image resolution are essentially relaxed.

This paper is organized as follows. In Section 2, techniques for constructing two-dimensional (2D) stochastic fracture networks and calculating fractal dimension and multifractal spectrum are introduced. In Section 3, impacts of different fracture geometrical properties on the fractal and multifractal patterns are presented. We then conduct a sensitivity analysis in Section 3, which quantifies the significance of each parameter on the fractal and multifractal patterns. To our knowledge, this is the first systematic analysis of the impact of geometrical properties of stochastic fractures – including fracture length, position, orientation and system size – on the fractal and multifractal characterization. Finally, conclusions are summarized in Section 4.

2. Materials and methods

This section introduces the method to construct stochastic fracture networks in 2D (two-dimensional) and calculate the single fractal dimension and multifractal spectrum with the box-counting method.

2.1. Construction of stochastic fracture networks

Real fracture networks are complex, and it is difficult to quantify their properties precisely. To reduce modeling complexity, line segments are used to represent fractures in 2D. The three geometrical parameters that describe each fracture are fracture lengths, orientations, and positions of the fracture centers. Each parameter can be characterized with a different statistical distribution.

The fracture lengths are characterized by a power-law distribution [28]

$$n(l) = \beta l^{-a}, \tag{1}$$

where $n(l)dl$ is the number of fractures with lengths ranging from $[l, l + dl]$, β is the coefficient of proportionality and a is the power-law exponent. Bour and

Davy [28] and Zhu et al. [24] showed that this exponent should range approximately from 2 to 3. The probability of generating very long fractures decreases sharply as a increases.

The fracture orientations follow von Mises–Fisher distributions [29, 30, 31]

$$f(\vec{x}, \vec{\mu}, \kappa) = C(\kappa) \exp(\kappa \vec{\mu}^T \vec{x}), \tag{2}$$

where $C(\kappa)$ is the normalization constant. $\vec{\mu}$ and κ are the mean direction and concentration parameter, respectively. In this research, we choose $\vec{\mu} = [1, 0]$ and κ of 0, 1, 5, 10. The parameter κ controls the concentration degree of the distribution around the mean direction $\vec{\mu}$. When $\kappa = 0$, the von Mises–Fisher distribution degenerates to a uniform distribution. When κ is large, the distribution is approximate to a normal distribution and concentrates around the angle $\vec{\mu}$ with $1/\kappa$ analogous to σ^2.

The positions of fracture centers are sampled from a uniform or fractal distribution. The fractal spatial density distribution [32, 33] introduces clustering effects in the network, which is characterized by a fractal dimension F_D. Darcel et al. [33] and Zhu et al. [24] showed that real fracture networks exhibit clustering effects.

Examples of different fracture networks in 2D are shown in Fig. 1. In this research, the formation of a spanning cluster is set as the termination criterion, not a prescribed fracture intensity [18]. A spanning cluster (red fractures in Fig. 1) connects all four sides of the domain boundary, which is the only pathway of fluid flow across the low-permeability system and represents good global connectivity. In contrast, fracture intensity is not a good indicator for connectivity because it is sensitive to fracture geometries, such as fracture lengths, orientations and clustering effects.

2.2. Fractal dimension and multifractal spectrum

A box-counting method superimposes grids with boxes of different sizes, r, on a fracture pattern and count the number of boxes containing fractures, N_r.

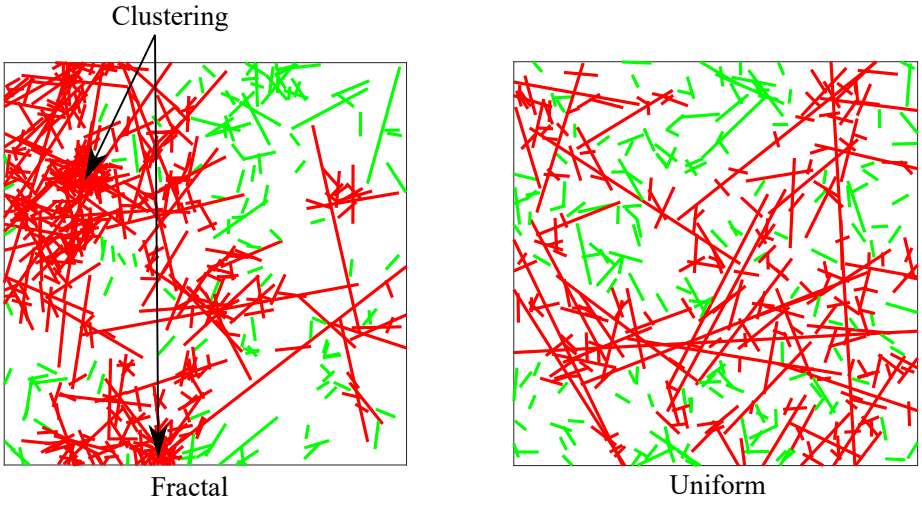

Figure 1: 2D fracture networks. The red line segments form the connected spanning cluster. The green line segments correspond to all other locally connected clusters. In both networks, the fracture orientations follow a uniform distribution, and lengths obey a power-law distribution. The **left** network has fracture center positions that follow a fractal spatial density distribution with the fractal dimension of 1.5, and in the **right** network, the fracture centers follow a uniform distribution.

For a fractal pattern, N_r and r fulfill the relation:

$$N_r = r^{-D}, \tag{3}$$

where D is the fractal dimension of the pattern. By fitting the $\ln(N_r)$ and $\ln(r)$ with a linear function, the slope is the corresponding fractal dimension. Fig. 2 demonstrates the process to cover the fracture network with boxes of different sizes.

The conventional box-counting method uses outcrop images, and its minimum box size is limited by the image resolution, which calculates inaccurate fractal dimensions [27]. For stochastic fracture networks in this work, each fracture is represented by a line segment, so the box size can be infinitely small, which is superior to the conventional method.

Fracture networks are usually composed of different sets of fractures. A single fractal dimension is insufficient to characterize the complexity of fracture

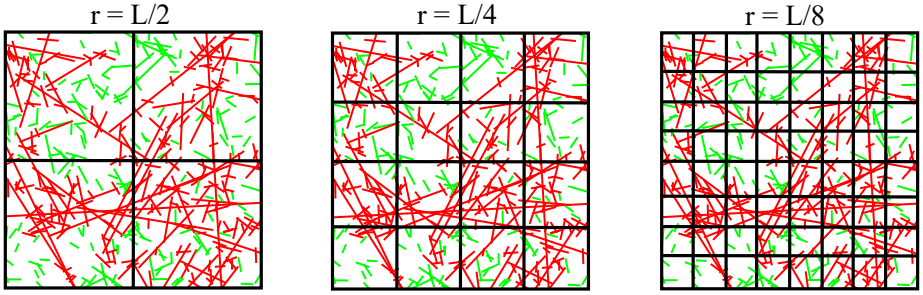

Figure 2: Demonstration of calculating the fractal dimension of a stochastic fracture network with the box-counting method.

networks. Instead, the multifractal spectrum is more suitable.

The procedure to obtain a multifractal spectrum through the box-counting method is as follows:

1. Define a probability distribution function for the fracture network:

$$p_i(r) = \frac{l_i}{\sum_{i=1}^{N} l_i}, \tag{4}$$

where l_i is the length of fractures in the box i, r is the size of the box, N is the number of fractures in the system.

2. Define a partition function [21], which is the summation of q^{th} power of the probability distribution function:

$$\chi_q(r) = \sum p_i(r)^q = r^{\tau(q)}, \tag{5}$$

where q is the probability moment order, which varies between $-\infty$ and $+\infty$ for a full spectrum. The negative q magnifies the importance of boxes with small p_i, while positive q stresses the importance of boxes with large p_i. $\tau(q)$ is a mass exponent. In practice, we choose q varying between $[-18, 18]$ with a step of 1. If r is small enough, $\tau(q)$ can be calculated by:

$$\tau(q) = \lim_{r \to 0} \frac{\ln(\chi_q(r))}{\ln(r)}, \tag{6}$$

3. Perform Legendre transform on $\tau(q)$ to get the multifractal spectrum $f(\alpha)$

$$\alpha = \frac{d\tau(q)}{dq} = \lim_{r \to 0} \frac{\sum_{i=1}^{N} p_i(r)^q \ln(p_i(r))}{\sum_{i=1}^{N} p_i(r)^q \ln(r)}, \tag{7}$$

$$f(\alpha) = \alpha q - \tau(q), \tag{8}$$

where α is the Lipschitz-Hölder exponent, reflecting the singularity of fractal subsets. $f(\alpha)$ is the multifractal spectrum, which describes the fractal dimension of subsets with different α values.

Applying numerical Legendre transom decreases the accuracy of the results. Therefore, averaging over several samples is highly beneficial [34]. In this research, we average results over ten independent realizations.

3. Results and discussions

We systematically investigate those geometrical properties, which are characterized by the essential parameter of their stochastic distributions. The power-law exponent (a) characterizes fracture lengths. The fractal dimension (F_D) of the spatial density distribution characterizes fracture positions. The concentration parameter (κ) in the von Mises–Fisher distribution characterizes orientations. We choose 11 values of the power-law exponent ($a \in [2.0, 3.0]$ with a step of 0.1), 9 of the fractal dimension ($F_D \in [1.2, 2.0]$ with a step of 0.1), 4 values of the concentration parameter ($\kappa = 0, 1, 5, 10$) and 3 values of the system size ($L = 10, 30, 50$). Each case with a given set of parameters is stabilized by averaging over ten independent realizations.

Seven decreasing box sizes are used for the box-counting method:

$$bs = \frac{L}{2^i}, \qquad i = 1, 2, 3, \ldots, 7 \tag{9}$$

where bs is the box size, and L is the system size.

Through a linear regression of $\ln(N(r))$ and $\ln(1/r)$, we obtain the single fractal dimension. The fractal dimension of the fracture network in Fig. 3(a) is 1.85, which is shown in Fig. 4(a). Parameters for the fracture network are $a = 2.5, F_D = 1.5, \kappa = 0$, and $L = 50$.

For multifractal spectrum, we test the linear relationship of Eq. 5 in a log-log plot for each case. Fig. 3 (b) and (c) exhibit the double-log plot of $\chi_q(r)$

and r and its correlation coefficient with different q values, respectively. Fig. 3 (c) shows that the correlation coefficient is either approximately 1 or -1 for different q. Therefore, the fracture network shows multifractal patterns and makes the following calculation of the multifractal spectrum possible. In Fig. 3 (b), when $q = 1$, $\chi_q(r) = 1$ for any box sizes and the slope is zero . When $q = 0$, $\chi_q(r) = N(r)$, the slope yields the reverse value of the single fractal dimension D. Fig. 4 (b) exhibits the multifractal spectrum of the fracture networks in Fig. 3 (a). $f(\alpha)$ is the fractal dimension of different subsets with the same α value, the largest value of $f(\alpha)$ is the single fractal dimension, referring to the fractal dimension of the most probable singularity subset within the whole fracture network. In this calculation, its value is 1.86, slightly larger than the 1.85 calculated before because of the inaccuracy caused by the numerical transform and the fact that fracture networks are not strict fractal sets but stochastic ones. Different α values refer to subsets with different singular degrees, and its variations, $\Delta\alpha$, is a good indicator of the system complexity. For the fracture network in Fig. 3(a), $\Delta\alpha$ equals 2.8.

Fig. 5 exhibits the cumulative distribution function of the single fractal dimension and $\Delta\alpha$, where the P_{10}, P_{50}, P_{90} estimates are denoted. There is a positive correlation between D and $\Delta\alpha$, shown in Fig. 5 (c), which means that both indicators can describe the complexity of fracture networks. However, their correlation is not strong enough to regard the two indicators as identical. The statistics of full datasets are summarized in Table. 1.

The following sections show the impact of different fracture geometry properties on the fractal and multifractal characterization. In particular, we choose the single fractal dimension, D, and variation, $\Delta\alpha$, to represent characteristics of the fractal and multifractal, respectively. We also select representative cases by controlling rest variables to stress the impact of each parameter. A summary of parameters used in this paper is listed in Table. 2 for clarification.

Table 1: Statistics of the single fractal dimension, D, and $\Delta\alpha$

Case	D	$\Delta\alpha$
Number of simulation	1,188	1,188
Max	1.974	3.146
Min	1.525	1.698
Mean	1.787	2.240
Median	1.798	2.191
Standard deviation	0.0924	0.257
P_{10}	1.653	1.949
P_{50}	1.798	2.191
P_{90}	1.902	2.619

Table 2: Summary of parameters in this paper

Parameter	Usage or Definition
a (power-law distribution)	Describing fracture lengths
F_D (fractal spatial density distribution)	Describing fracture center positions
κ (von Mises–Fisher distribution)	Describing fracture orientations
L (system size)	Descrbing system sizes
D	Single fractal dimension
$\Delta\alpha$	Difference of the Lipschitz-Hölder exponent α

Table 3: Three levels of each parameter

Parameter	Low	Intermediate	High
a	2.0	2.5	3.0
F_D	1.2	1.6	2.0
κ	0	5	10
L	10	30	50

3.1. Impact of fracture geometries on the single fractal dimension

Figs. 6, 7, 8 and 9 show the impact of fracture length (a), positions (F_D), orientations (κ) and system size (L) on the single fractal dimension (D), respectively. For each target parameter, nine scenarios with different combinations of the rest three parameters are presented to demonstrate the correlation with the single fractal dimension. We conduct a Taguchi design [35] and use a three-level L_9 orthogonal array to design the combinations of parameters, which can effectively eliminate the repetition of combinations. The correlation coefficient of each scenario is denoted in the figure. For each parameter, we select three levels (Low, Intermediate, High) to present the results, which are listed in Table. 3.

The power-law exponent, a (Fig. 6), concentration parameter, κ (Fig. 8), and system size, L (Fig. 9) have positive correlations with the single fractal dimension, D. This indicates that a large fracture network composed of small fractures with concentrated orientations yields a large fractal dimension. The mean values of the correlation coefficients for each parameter are 0.90, 0.94 and 0.97, respectively. Therefore, the system size is the most significant parameter to the single fractal dimension. However, F_D has a weak correlation with the single fractal dimension, D, indicating that clustering effects do not significantly change the fractal dimension. In other words, the single fractal dimension cannot capture the complexity caused by clustering effects.

3.2. Impact of fracture geometries on multifractal spectrum

Figs. 10, 11, 12 and 13 show the impact of fracture length (a), positions (F_D), orientations (κ) and system size (L) on $\Delta\alpha$ of the multifractal spectrum,

respectively. For each target parameter, the same Taguchi design is implemented and 9 scenarios are presented for the demonstration.

The power-law exponent, a (Fig. 10), concentration parameter, κ (Fig. 12), and system size, L (Fig. 13), have positive correlations with $\Delta\alpha$. The mean values of correlation coefficients for each parameter are 0.65, 0.58 and 0.87, respectively. Therefore, the system size has the most significant impact on $\Delta\alpha$. F_D has a strong negative correlation with $\Delta\alpha$, indicating that clustering effects change $\Delta\alpha$ significantly. Clusters make fracture network more complex and cause $\Delta\alpha$ increase. Therefore, a multifractal spectrum can capture the complexity caused by clustering effects. However, the correlations of a, κ and L are not as strong as the single fractal dimension cases because all four parameters contribute to $\Delta\alpha$, and F_D has a negative correlation, which counteracts the positive correlation of these three parameters.

3.3. Sensitivity analysis

In this section, we perform a sensitivity analysis to explore the impact of each geometrical parameter on fractal and multifractal characterizations with the complete datasets.

We adopt the input/output correlation method, in which the sensitivity of model response Y to the components of the input random vector X is calculated by determining the component-wise correlation coefficients between these two vectors. Consider n samples of the input random vector $X = \{x^{(1)}, x^{(2)}, x^{(3)}, \ldots, x^{(n)}\}$, and the corresponding model responses $Y = \{y^{(1)}, y^{(2)}, y^{(3)}, \ldots, y^{(N)}\}$. The linear correlation coefficient ρ_i between the i^{th} input and output is defined as

$$\rho_i = \rho(X_i, Y) = \frac{E[(X_i - \mu_i)(Y - \mu_Y)]}{\sigma_i \sigma_Y}, \tag{10}$$

where μ_i and μ_Y are the expected values of X_i and Y respectively, and σ_i and σ_Y are the corresponding standard deviations.

The importance of each factor is ranked based on the correlation coefficient. The response is the single fractal dimension and $\Delta\alpha$ value of the multifractal spectrum. The input vector includes a, F_D, L, and κ. Fig. 14 shows the

sensitivity analysis between the geometrical parameters and the fractal and multifractal responses. For the single fractal dimension, fracture positions (F_D) shows a negligible correlation with the response, in agreement with the observations in the previous section. It indicates that a single fractal dimension cannot distinguish differences caused by clustering effects. The exponent a exhibits a positive correlation, which means that fracture networks with more small fractures have larger fractal dimensions. The system size L has the largest positive correlation coefficient among the four parameters. Therefore, it has the greatest impact on the fractal dimension, possibly attributing to the fact that a larger system has more different fractures described by fracture lengths and orientations. This observation does not contradict the definition of fractal sets, where their complexity should be independent of the scale. A larger system does not eliminate small fractures, and system sizes here are at the same scale with the same order of magnitude. The concentration parameter κ has a large positive correlation, indicating that fracture networks with more concentrated orientations have larger fractal dimensions. In this research, the termination criterion of a fracture network is the formation of a spanning cluster. Therefore, for a fracture network with more concentrated orientations, more fractures are required to form a spanning cluster, making the fracture network more complex and corresponds to a larger fractal dimension.

For $\Delta\alpha$ value of the multifractal spectrum, clustering effects have a strong negative correlation, which indicates that the clustering effect can enlarge $\Delta\alpha$'s value and increase the complexity of fracture networks. The system size L has the most significant positive correlation coefficient, and the exponent a and concentration κ have positive correlation coefficients. The correlation coefficients of a, κ and L are smaller than those of the single fractal dimension, consistent with the observations in the previous section.

3.4. Real fracture networks and their fractal and multifractal characterization

By applying the pixel-based fracture detection algorithm [26], we can digitize published fracture outcrop maps quickly. The algorithm tracks all fracture

trace pixels and uses line segments or polylines to represent a fracture. Therefore, the limit on the box size is relaxed. We have digitized 60 outcrop images from different publications. Their scales range from millimeters to thousands of kilometers [36, 37, 38, 17, 39, 40, 41, 42].

From testing the linear relationship of Eq. 3 and Eq. 5 in a log-log plot, natural fracture outcrop maps show fractal and multifractal patterns. Fig. 15(a) shows the fractal dimensions of these outcrops, which vary between 1.32 and 1.93 with a mean value of 1.67. Fig. 15(b) shows values of $\Delta\alpha$ in different outcrops varying between 0.99 and 1.91 with a mean value of 1.52. The non-zero value of $\Delta\alpha$ suggests that natural fracture networks can never be a homogeneous monofractal set at any scales. Both D and $\Delta\alpha$ values have smaller means than stochastic fracture networks. This indicates that stochastic fracture networks have more complex structures than natural outcrops, attributing to various fracture lengths, orientations, clustering effects and usually higher fracture intensities.

Furthermore, at a similar scale, different outcrops have significant variations on D and $\Delta\alpha$, revealing that natural fracture networks are extremely complex depending on their geological history, environment and rock types. It is unlikely to find a universal indicator, which can characterize the complexity of fracture networks at different scales or the same scale. Both D and $\Delta\alpha$ have weak correlations with scales (-0.10 and -0.12, respectively). This indicates that the complexity of fracture networks is indeed independent of scales, which supports the argument that natural fracture networks have self-similarity patterns.

Fig. 15(c) shows the correlation between the single fractal dimension and $\Delta\alpha$. The correlation coefficient is 0.04, indicating almost no correlation between these two indicators. Therefore, in natural outcrops, the single fractal dimension and the multifractal spectrum are almost independent. This observation is different from the behavior of D and $\Delta\alpha$ in stochastic fracture networks, where they have positive correlations. One possible reason for the inconsistent behavior is that stochastic fracture networks have over-simplifications on fracture geometries. Although stochastic fractures have more complex structures

regarding fracture intensities, lengths, orientations and clustering effects, and they have larger values of fractal dimension and $\Delta\alpha$, they neglect several important fracture geometries, such as the fracture tortuosity and T-type intersections between fractures. Tortuosity may not be significant for the macro-scale connectivity of fracture networks; however, T-type intersections are essential because they reduce dead-ends in the system and enhance connectivity [43, 44]. The other possible reason is the clustering effects. Clustering effects are commonly observed from outcrops [15, 24]. From the analysis in the previous section, the single fractal dimension is insensitive to the clustering effects, while $\Delta\alpha$ is sensitive. Therefore, it is superior to describe the complexity of fracture networks with $\Delta\alpha$ instead of the single fractal dimension D. Natural fracture networks show nontrivial multifractal patterns, and the multifractal spectrum can better describe the complex fracturing mechanisms and geological formation heterogeneity [45, 46].

4. Conclusions

In this research, we systematically analyze the impact of different geometrical properties (a, F_D, κ, L) of fracture networks on their fractal and multifractal characterizations. The key conclusions of this study are:

1. In stochastic fracture networks, a single fractal dimension and $\Delta\alpha$ of the multifractal spectrum can evaluate the complexity of fracture networks. They are positively correlated with a correlation coefficient of 0.65.
2. Fracture lengths (a), orientations (κ), and system sizes (L) have positive correlations with the single fractal dimension and $\Delta\alpha$. The system size has the most significant impact among these four parameters.
3. The single fractal dimension cannot capture the complexity caused by clustering effects; therefore, F_D has a weak correlation with D.
4. $\Delta\alpha$ is superior to D in characterizing the complexity of fracture networks. It has a strong negative correlation with F_D, which means that clustering

effects make fracture networks more complex, and $\Delta\alpha$ can capture the difference.

5. Our fracture detection algorithm digitizes 60 real outcrop maps with scales ranging from millimeters to kilometers. The single fractal dimension and $\Delta\alpha$ have wide variations in those outcrops. However, both indicators have smaller mean values than stochastic fracture networks, indicating a less complex structure in natural outcrops.
6. Both indicators have wide variations in outcrops of similar scales, indicating real fracture networks are complex due to their geological history, environment and rock types. It is almost impossible to find a universal indicator that can characterize the complexity of fracture networks at different scales or the same scale, which also supports the self-similarity patterns of natural fracture networks.
7. Inconsistent behaviors of D and $\Delta\alpha$ in stochastic fracture networks and natural outcrop maps indicate that stochastic fracture networks may have over-simplifications on fracture geometries. More realistic fracture networks incorporating fracture tortuosity and T-type intersections should be developed for further investigations.

Data Availability

All the synthetically generated data are available online (https://doi.org/10.4121/14464893)

Declaration of Competing Interest

The authors declare that they have no known competing financial interests or personal relationships that could have appeared to influence the work reported in this paper.

Acknowledgments

This project was supported by the National Key Research and Development Program of China (No. 2019YFA0708704). The authors would like to thank all

editors and anonymous reviewers for their comments and suggestions.

References

[1] M. H. Anders, S. E. Laubach, C. H. Scholz, Microfractures: A review, Journal of Structural Geology 69 (2014) 377–394.

[2] M. D. Zoback, S. M. Gorelick, Earthquake triggering and large-scale geologic storage of carbon dioxide, Proceedings of the National Academy of Sciences 109 (2012) 10164–10168.

[3] A. G. Fountain, R. W. Jacobel, R. Schlichting, P. Jansson, Fractures as the main pathways of water flow in temperate glaciers, Nature 433 (2005) 618–621.

[4] S. Follin, L. Hartley, I. Rhén, P. Jackson, S. Joyce, D. Roberts, B. Swift, A methodology to constrain the parameters of a hydrogeological discrete fracture network model for sparsely fractured crystalline rock, exemplified by data from the proposed high-level nuclear waste repository site at Forsmark, Sweden, Hydrogeology Journal 22 (2014) 313–331.

[5] K. Watanabe, H. Takahashi, Fractal geometry characterization of geothermal reservoir fracture networks, Journal of Geophysical Research: Solid Earth 100 (1995) 521–528.

[6] B. Berkowitz, Characterizing flow and transport in fractured geological media: A review, Advances in Water Resources 25 (2002) 861–884.

[7] B. B. Mandelbrot, Fractals: form, chance, and dimension, volume 706, WH Freeman San Francisco, 1977.

[8] K. Otsuki, T. Dilov, Evolution of hierarchical self-similar geometry of experimental fault zones: Implications for seismic nucleation and earthquake size, Journal of Geophysical Research: Solid Earth 110 (2005).

[9] X. Shi, J. Pan, Q. Hou, Y. Jin, Z. Wang, Q. Niu, M. Li, Micrometer-scale fractures in coal related to coal rank based on micro-ct scanning and fractal theory, Fuel 212 (2018) 162–172.

[10] H. Wu, Y. Zhou, Y. Yao, K. Wu, Imaged based fractal characterization of micro-fracture structure in coal, Fuel 239 (2019) 53–62.

[11] P. G. Okubo, K. Aki, Fractal geometry in the san andreas fault system, Journal of Geophysical Research: Solid Earth 92 (1987) 345–355.

[12] N. Matsumoto, K. Yomogida, S. Honda, Fractal analysis of fault systems in japan and the philippines, Geophysical Research Letters 19 (1992) 357–360.

[13] C. Aviles, C. Scholz, J. Boatwright, Fractal analysis applied to characteristic segments of the San Andreas fault, Journal of Geophysical Research: Solid Earth 92 (1987) 331–344.

[14] G. Cello, Fractal analysis of a quaternary fault array in the central apennines, italy, Journal of Structural Geology 19 (1997) 945–953.

[15] C. C. Barton, Fractal analysis of scaling and spatial clustering of fractures, in: Fractals in the earth sciences, Springer, 1995, pp. 141–178.

[16] J. Walsh, J. Watterson, Fractal analysis of fracture patterns using the standard box-counting technique: valid and invalid methodologies, Journal of structural Geology 15 (1993) 1509–1512.

[17] P. Gillespie, C. Howard, J. Walsh, J. Watterson, Measurement and characterisation of spatial distributions of fractures, Tectonophysics 226 (1993) 113–141.

[18] B. Berkowitz, A. Hadad, Fractal and multifractal measures of natural and synthetic fracture networks, Journal of Geophysical Research: Solid Earth 102 (1997) 12205–12218.

[19] B. B. Mandelbrot, The fractal geometry of nature, volume 1, WH freeman New York, 1982.

[20] U. Frisch, G. Parisi, Fully developed turbulence and intermittency, New York Academy of Sciences, Annals 357 (1980) 359–367.

[21] T. C. Halsey, M. H. Jensen, L. P. Kadanoff, I. Procaccia, B. I. Shraiman, Fractal measures and their singularities: The characterization of strange sets, Physical review A 33 (1986) 1141.

[22] P. A. Cowie, D. Sornette, C. Vanneste, Multifractal scaling properties of a growing fault population, Geophysical Journal International 122 (1995) 457–469.

[23] Q. Lei, J.-P. Latham, C.-F. Tsang, The use of discrete fracture networks for modelling coupled geomechanical and hydrological behaviour of fractured rocks, Computers and Geotechnics 85 (2017) 151–176.

[24] W. Zhu, S. Khirevich, T. Patzek, Percolation Properties of Stochastic Fracture Networks in 2D and Outcrop Fracture Maps, in: 80th EAGE Conference and Exhibition 2018, 2018.

[25] W. Zhu, B. Yalcin, S. Khirevich, T. Patzek, Correlation analysis of fracture intensity descriptors with different dimensionality in a geomechanics-constrained 3d fracture network, in: Petroleum Geostatistics 2019, volume 2019, European Association of Geoscientists & Engineers, 2019, pp. 1–5.

[26] W. Zhu, S. Khirevich, T. Patzek, Fracture recognition with u-net and pixel-based automatic fracture detection, in: Fourth Naturally Fractured Reservoir Workshop, volume 2020, European Association of Geoscientists & Engineers, 2020, pp. 1–5.

[27] A. Roy, E. Perfect, W. M. Dunne, L. D. McKay, Fractal characterization of fracture networks: An improved box-counting technique, Journal of Geophysical Research: Solid Earth 112 (2007).

[28] O. Bour, P. Davy, Connectivity of random fault networks following a power law fault length distribution, Water Resources Research 33 (1997) 1567–1583.

[29] J.-J. Song, C.-I. Lee, M. Seto, Stability analysis of rock blocks around a tunnel using a statistical joint modeling technique, Tunnelling and underground space technology 16 (2001) 341–351.

[30] J. Kemeny, R. Post, Estimating three-dimensional rock discontinuity orientation from digital images of fracture traces, Computers & Geosciences 29 (2003) 65–77.

[31] A. E. Whitaker, T. Engelder, Characterizing stress fields in the upper crust using joint orientation distributions, Journal of Structural Geology 27 (2005) 1778–1787.

[32] P. Meakin, Invasion percolation on substrates with correlated disorder, Physica A: Statistical Mechanics and its Applications 173 (1991) 305–324.

[33] C. Darcel, O. Bour, P. Davy, J. De Dreuzy, Connectivity properties of two-dimensional fracture networks with stochastic fractal correlation, Water resources research 39 (2003).

[34] H. Salat, R. Murcio, E. Arcaute, Multifractal methodology, Physica A: Statistical Mechanics and its Applications 473 (2017) 467–487.

[35] R. K. Roy, Design of experiments using the Taguchi approach: 16 steps to product and process improvement, John Wiley & Sons, 2001.

[36] M. Holland, N. Saxena, J. L. Urai, Evolution of fractures in a highly dynamic thermal, hydraulic, and mechanical system-(ii) remote sensing fracture analysis, jabal shams, oman mountains, GeoArabia 14 (2009) 163–194.

[37] K. Bisdom, Burial-related fracturing in sub-horizontal and folded reservoirs: Geometry, geomechanics and impact on permeability (2016).

[38] P. Segall, D. D. Pollard, Nucleation and growth of strike slip faults in granite, Journal of Geophysical Research: Solid Earth 88 (1983) 555–568.

[39] A. Jafari, Permeability estimation of fracture networks (2011).

[40] N. E. Odling, Scaling and connectivity of joint systems in sandstones from western norway, Journal of Structural Geology 19 (1997) 1257–1271.

[41] S. T. Thiele, L. Grose, A. Samsu, S. Micklethwaite, S. A. Vollgger, A. R. Cruden, Rapid, semi-automatic fracture and contact mapping for point clouds, images and geophysical data, Solid Earth 8 (2017) 1241–1253.

[42] L. Bertrand, Y. Géraud, E. Le Garzic, J. Place, M. Diraison, B. Walter, S. Haffen, A multiscale analysis of a fracture pattern in granite: A case study of the tamariu granite, catalunya, spain, Journal of Structural Geology 78 (2015) 52–66.

[43] P. Davy, R. Le Goc, C. Darcel, A model of fracture nucleation, growth and arrest, and consequences for fracture density and scaling, Journal of Geophysical Research: Solid Earth 118 (2013) 1393–1407.

[44] D. J. Sanderson, C. W. Nixon, The use of topology in fracture network characterization, Journal of Structural Geology 72 (2015) 55–66.

[45] P. A. Cowie, D. Sornette, C. Vanneste, Multifractal scaling properties of a growing fault population, Geophysical Journal International 122 (1995) 457–469.

[46] G. Ouillon, C. Castaing, D. Sornette, Hierarchical geometry of faulting, Journal of Geophysical Research: Solid Earth 101 (1996) 5477–5487.

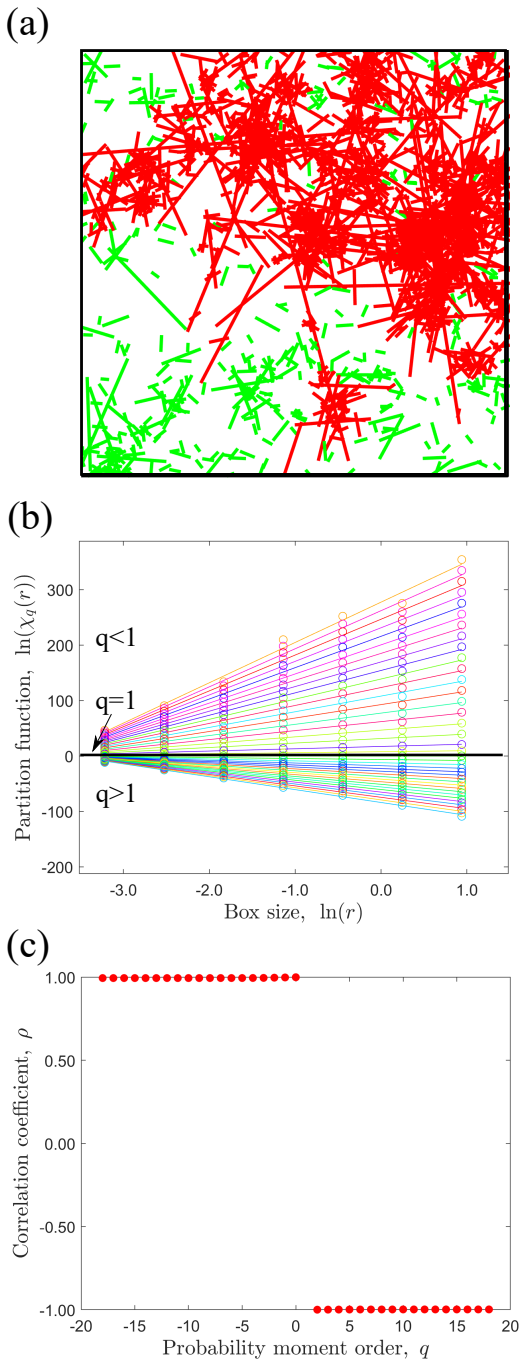

Figure 3: (a) A stochastic fracture network with $a = 2.5, F_D = 1.5, \kappa = 0$, and $L = 50$ (b) Log-log plot of $\chi_q(r)$ and r. Each line segment is a linear fit of the corresponding scatter points of the same color. (c) Correlation coefficient of each linear fit in (b) with respect to a different q

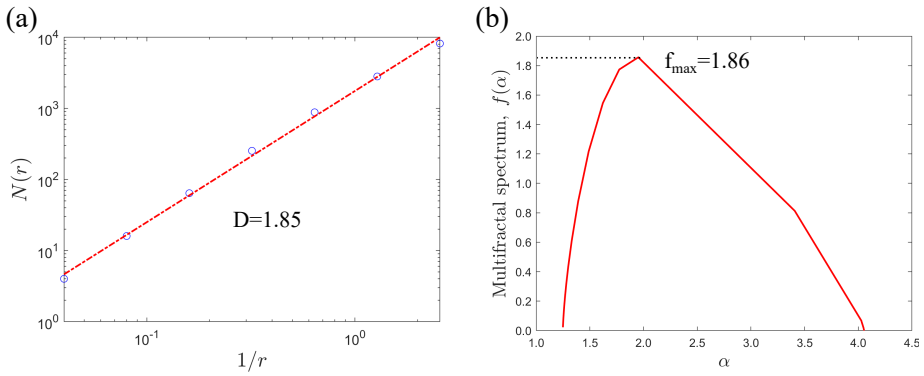

Figure 4: (a) Single fractal dimension, D; (b) multifractal spectrum of the fracture network in Fig. 3(a)

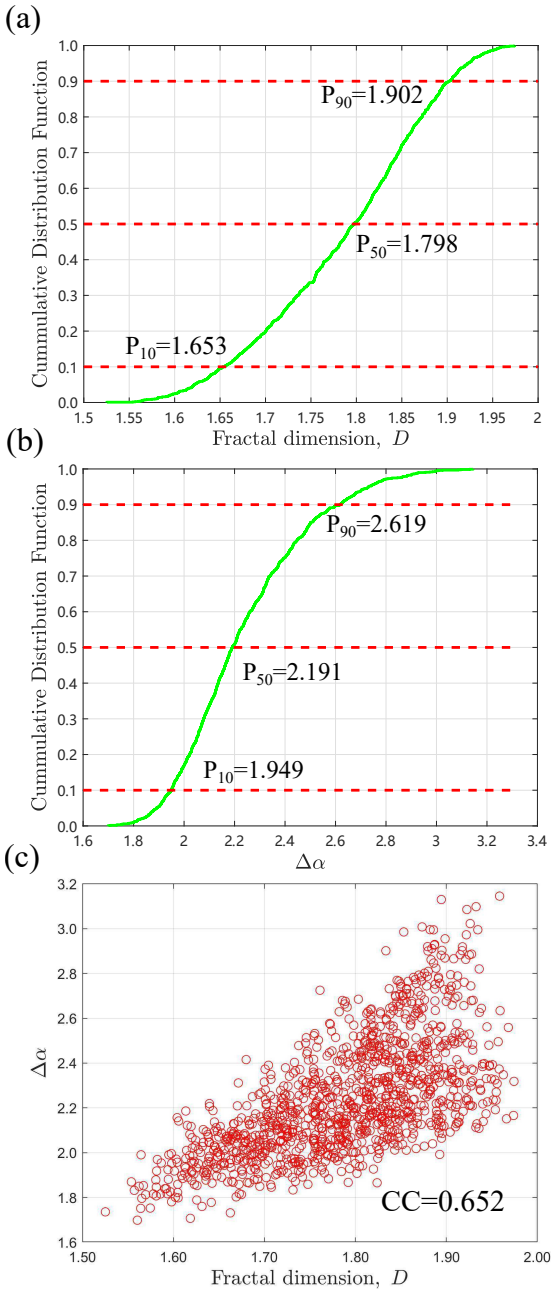

Figure 5: The cumulative distribution function of (a) the single fractal dimension, D, (b) $\Delta\alpha$, and (c) the correlation between D and $\Delta\alpha$

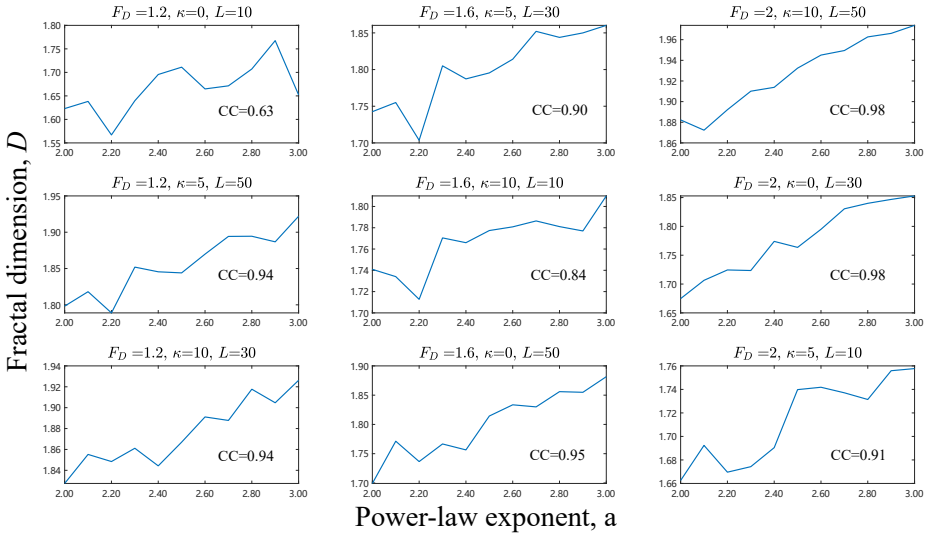

Figure 6: Impact of fracture lengths on the single fractal dimension, D. CC is the correlation coefficient of each scenario. Combinations of F_D, κ and L are determined by a Taguchi design with an L_9 orthogonal array.

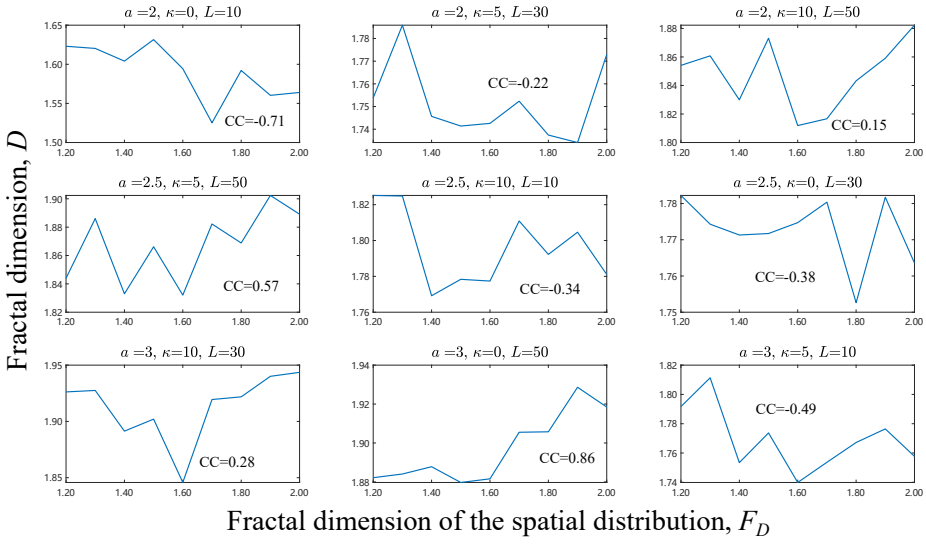

Figure 7: Impact of clustering effects on the single fractal dimension, D

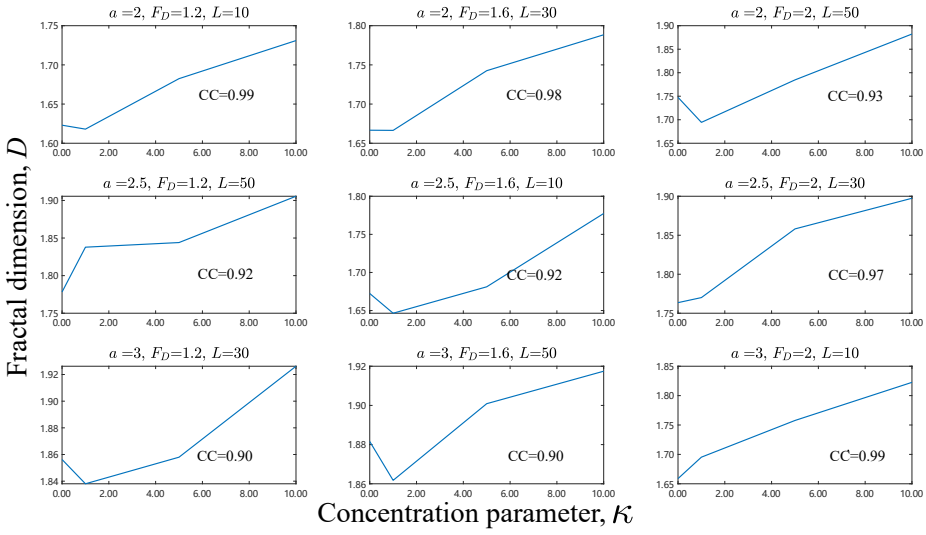

Figure 8: Impact of fracture orientations on the single fractal dimension, D

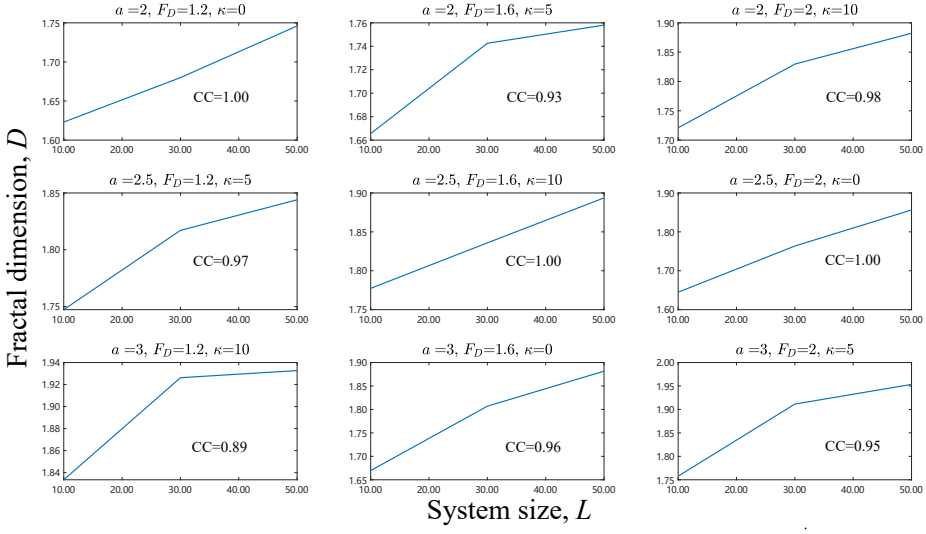

Figure 9: Impact of system sizes on the single fractal dimension, D

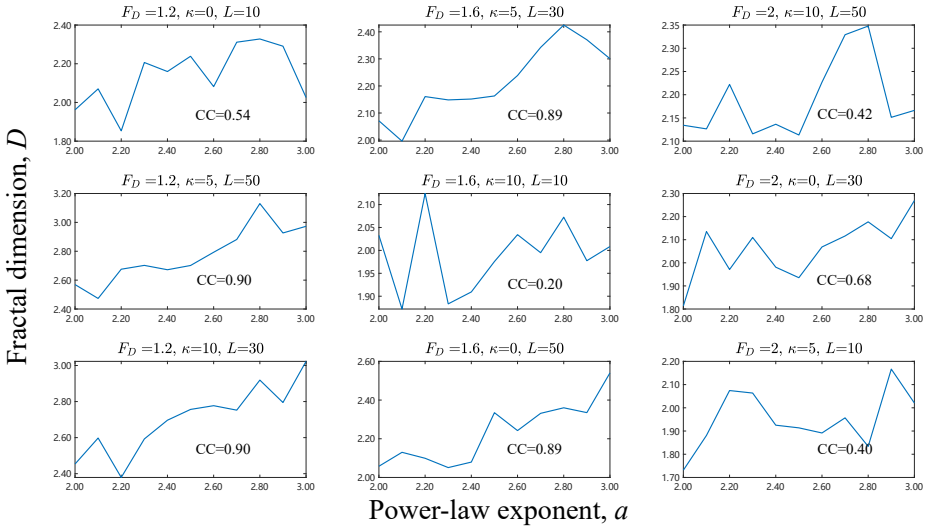

Figure 10: Impact of fracture lengths on $\Delta\alpha$

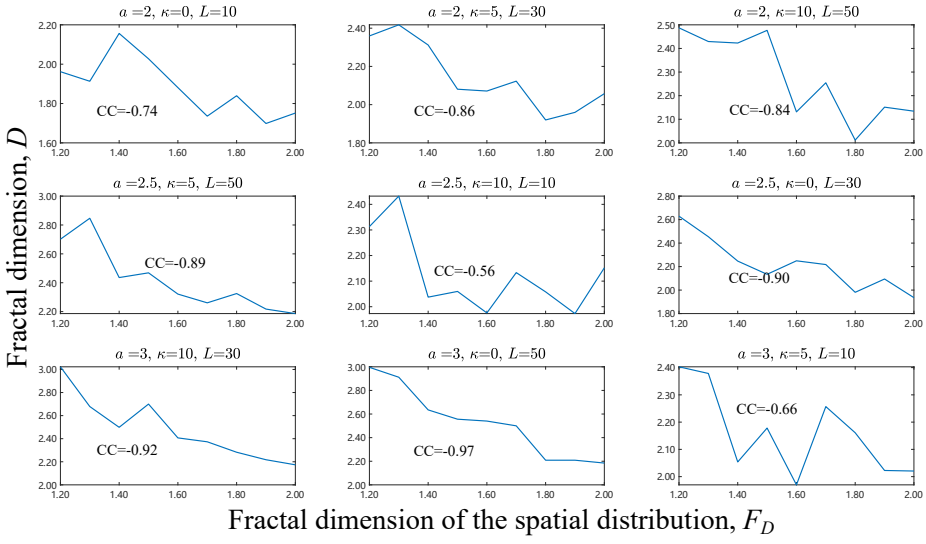

Figure 11: Impact of clustering effects on $\Delta\alpha$

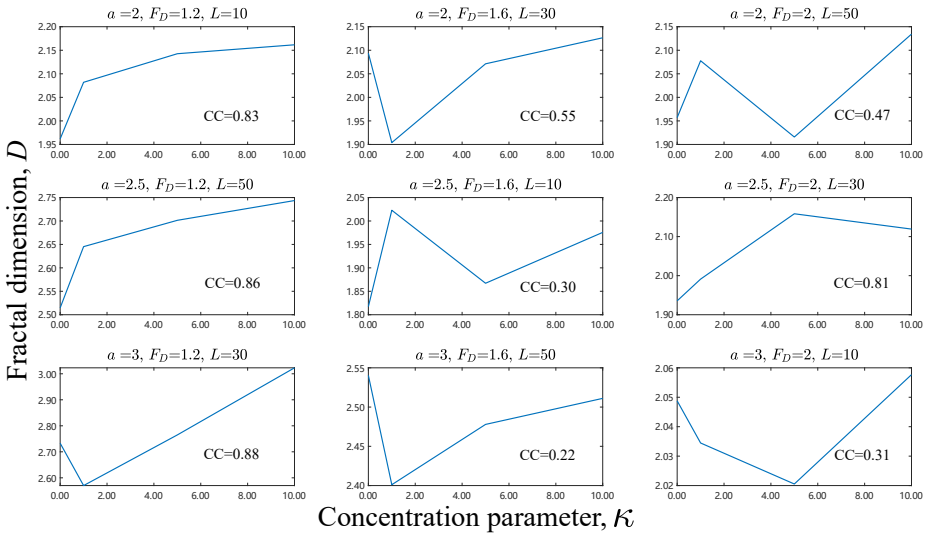

Figure 12: Impact of fracture orinetations on $\Delta\alpha$

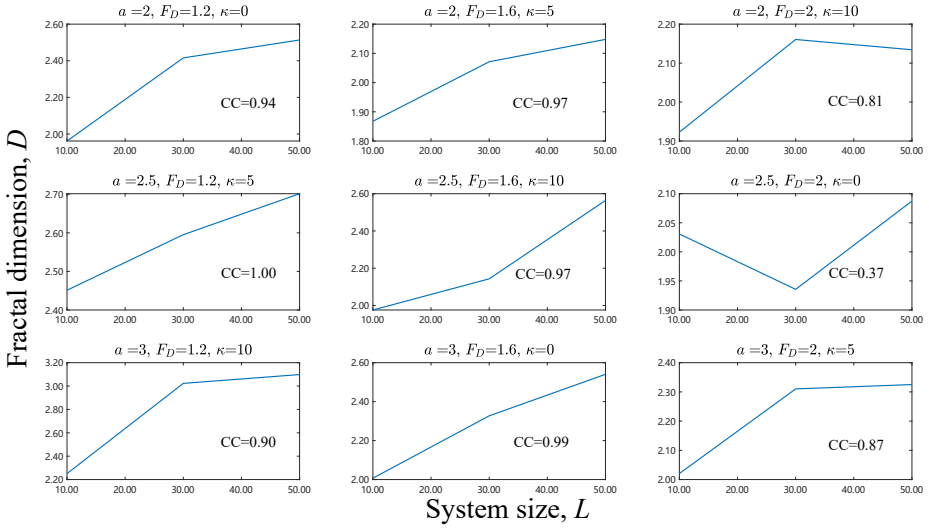

Figure 13: Impact of system sizes on $\Delta\alpha$

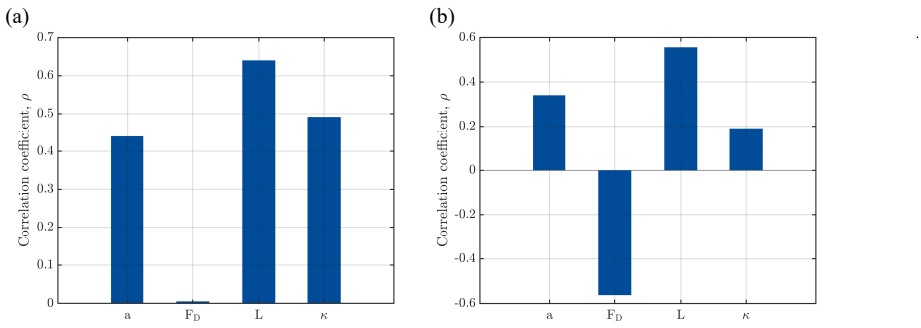

Figure 14: Linear correlation coefficient between each factor and the response (a: Fractal dimension, b: multifractal $\Delta\alpha$)

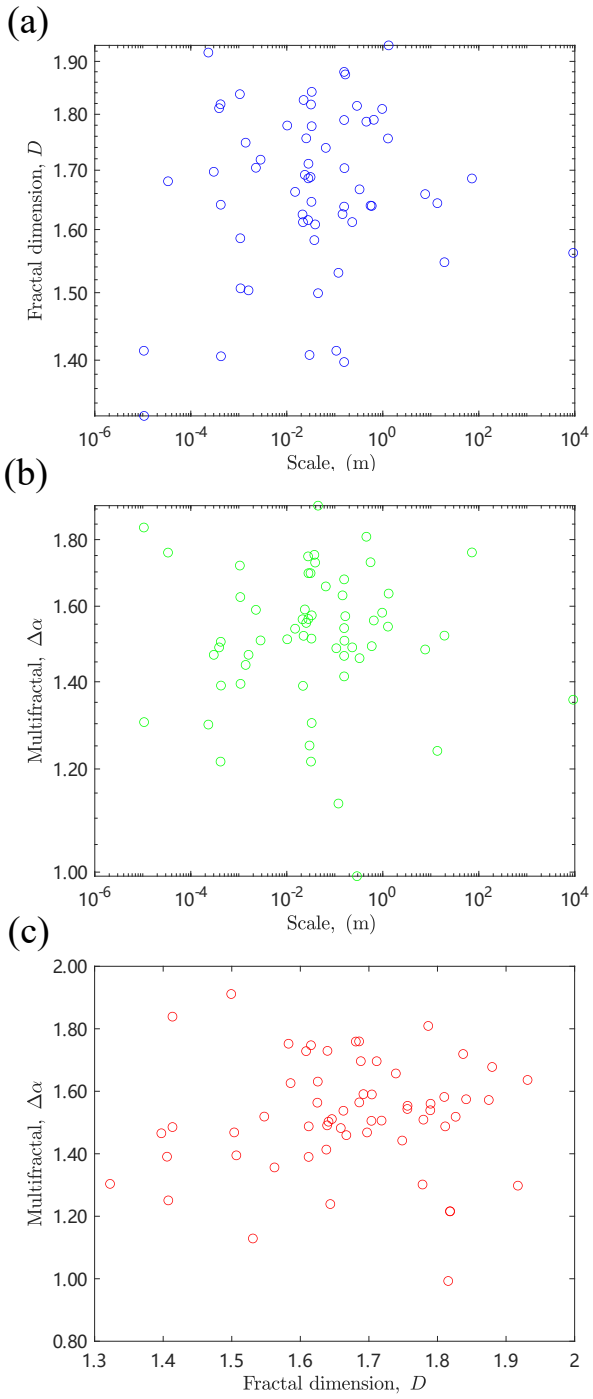

Figure 15: (a) Fractal dimensions, (b) $\Delta\alpha$ of fracture outcrops at different scales, and (c) correlation between the fractal dimension and $\Delta\alpha$